JOURNAL OF COMPUTATIONAL PHYSICS 70, 271–283 (1987)

Cavity Flow Dynamics at Higher Reynolds Number and Higher Aspect Ratio*

K. GUSTAFSON

Department of Mathematics, University of Colorado, Boulder, Colorado 80309

AND

K. HALASI

Department of Mathematics, Kansas State University, Manhattan, Kansas 66506

Received December 30, 1985; revised July 1, 1986

A primitive variable unsteady viscous incompressible Navier–Stokes flow simulation in a higher aspect ratio ($A = \text{depth/width} = 2$) driven cavity at a higher Reynold's number ($\text{Re} = 10{,}000$) exhibits dynamical features not apparent in previous studies of stationary solutions or at lower Reynold's number or in the more usual unit cavity investigations. The initial dynamics, e.g., between $t = 0$ sec and $t = 70$ sec, reveals transient bifurcations between states including two, three, and four interacting vortices in an interior separation region. Following this, there is an intermediate interval, e.g., between $t = 70$ sec and $t = 140$ sec, characterized by a vertical oscillation of the primary vortex related to the general activities of the secondary features of the flow. The long time behavior, e.g., between $t = 140$ seconds and $t = 360$ seconds, is one of qualitative smoothing of all secondary features except a persistent oscillation indicating a Hopf bifurcation.

1. INTRODUCTION

In a previous paper [1] we presented a comprehensive study of the unsteady flow dynamics of two-dimensional driven cavity flow. Differentiation of flow characteristics in terms of both the Aspect Ratio $A = \text{depth/width}$ and the Reynolds number $\text{Re} = 1/\text{viscosity}$ were investigated in [1] for A between $\frac{1}{2}$ and 4 and for Re between 10^{-6} and 2000. We also investigated some cavities deeper than $A = 4$, e.g., $A = 5$ and 6, but quickly found that these more expensive runs revealed no essential new flow features beyond what is seen already at depth $A = 2$.

Because deep cavity (here, $A = 2$) flow dynamics were seen in [1] to be far more interesting than those of the more usual unit cavity ($A = 1$) investigations (see [1] for an account of such recent studies), we decided to simulate the full flow dynamics at $A = 2$ at the higher Reynolds number $\text{Re} = 10{,}000$. Using a time interval

* Partially supported by a computing resources NCAR Grant 35071080. The authors gratefully acknowledge use of the CRAY 1 for these studies.

0021-9991/87 $3.00

$\Delta t = 0.001$ the flow exhibited an interesting initial transient dynamics, from $t = 0$ sec to $t = 70$ sec, not seen before. These results are described in Section 3. After these initial transients, it appeared that all qualitative features of flow had established themselves. There followed, until about $t = 140$ sec, an interval marked by a vertical oscillation in the position of the principal vortex. The flow during this intermediate interval is described in Section 4.

Thereafter, we were tempted at $t = 180$ sec to terminate the simulation, accepting that from most indications the flow was converging to a final steady state. Such final steady states had been achieved in all of the unsteady flows studied in [1]. However, because there remained a persistent secondary oscillation, qualitatively localized mainly to an ongoing interaction between a left wall vortex and a left corner vortex, we continued the flow beyond $t = 180$ sec to $t = 360$ sec. The oscillation, which could represent a Hopf bifurcation, remained. This final behavior is described in Section 5.

2. Some Flow Simulation Details

We refer to [1] for a full general description of the cavity problem treated and a comparative account of a number of recent cavity flow studies and the numerical schemes employed. In the present study, attention was focused entirely on the case of a cavity of width 1 and depth 2. In this cavity the viscous incompressible Navier–Stokes equations

$$V_t - \frac{1}{\mathrm{Re}} \Delta V + (V \cdot \nabla) V = -\nabla P \tag{2.1}$$

$$\nabla \cdot V = 0 \tag{2.2}$$

were discretized, following [1], on a uniform 40×80 grid using a modified MAC (marker and cell) staggered mesh scheme. See [2] for a good account of MAC schemes, the related projection and fractional step methods, and boundary value considerations. The flow was generated from an impulsive start and continued thereafter by a continuously moving top lid. See Fig. 1.

Briefly, see [1], the flow is advanced alternately between the velocity V^n and the pressure P^{n+1} by means of the pressure equation

$$\Delta P^{n+1} = -\operatorname{div}((V^n \cdot \nabla) V^n) \tag{2.3}$$

with boundary condition

$$n \cdot \nabla P^{n+1} = \frac{1}{\mathrm{Re}} n \cdot \Delta V^n. \tag{2.4}$$

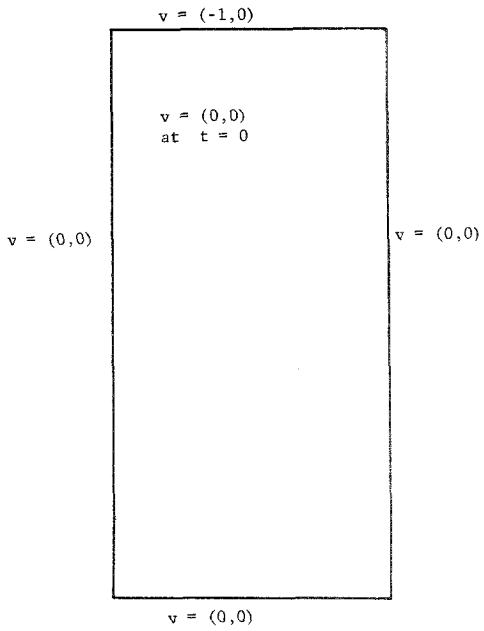

FIG. 1. Driven cavity, aspect ratio $A = 2$.

In the velocity advancement there is an intermediate predictor–corrector step, see [1] or [2], an effect of which is to ensure that each V^{n+1} is discretely incompressible.

As mentioned in [1], in preliminary experiments, we found no computational advantages of an implicit method over forward Euler, and hence used the latter for advancing the velocity in time.

Underlying the use of (2.3) and (2.4) are assumptions that the analytic momentum equation (2.1) possesses solutions (v, p) smooth enough so that one can differentiate Eq. (2.1), continue it to the boundary, and still retain a consistent discretization thereafter.

For convergence of such computations and accuracy at initial and intermediate times it is important [3] that the initial data $V(0)$ be weakly solenoidal. Note that this is the case for the driven cavity initial data and discretizations that we employed.

Rather than (2.4) one can actually set $\partial p/\partial n = 0$ on the boundary and eventually expect good results. See, for example, [3, Chap. III, Sect. 7.11 and Remark 7.2], where $\partial P^{n+1}/\partial n = 0$ at each time step and yet P^{n+1} and V^{n+1} converge. No upwinding was used, so that the numerical flow transients could be accurately portrayed. See Section 6 for comments on stability of the scheme.

In all figures we have normalized the velocity vectors to provide better visualization of the qualitative, rather than quantative, features of the flow.

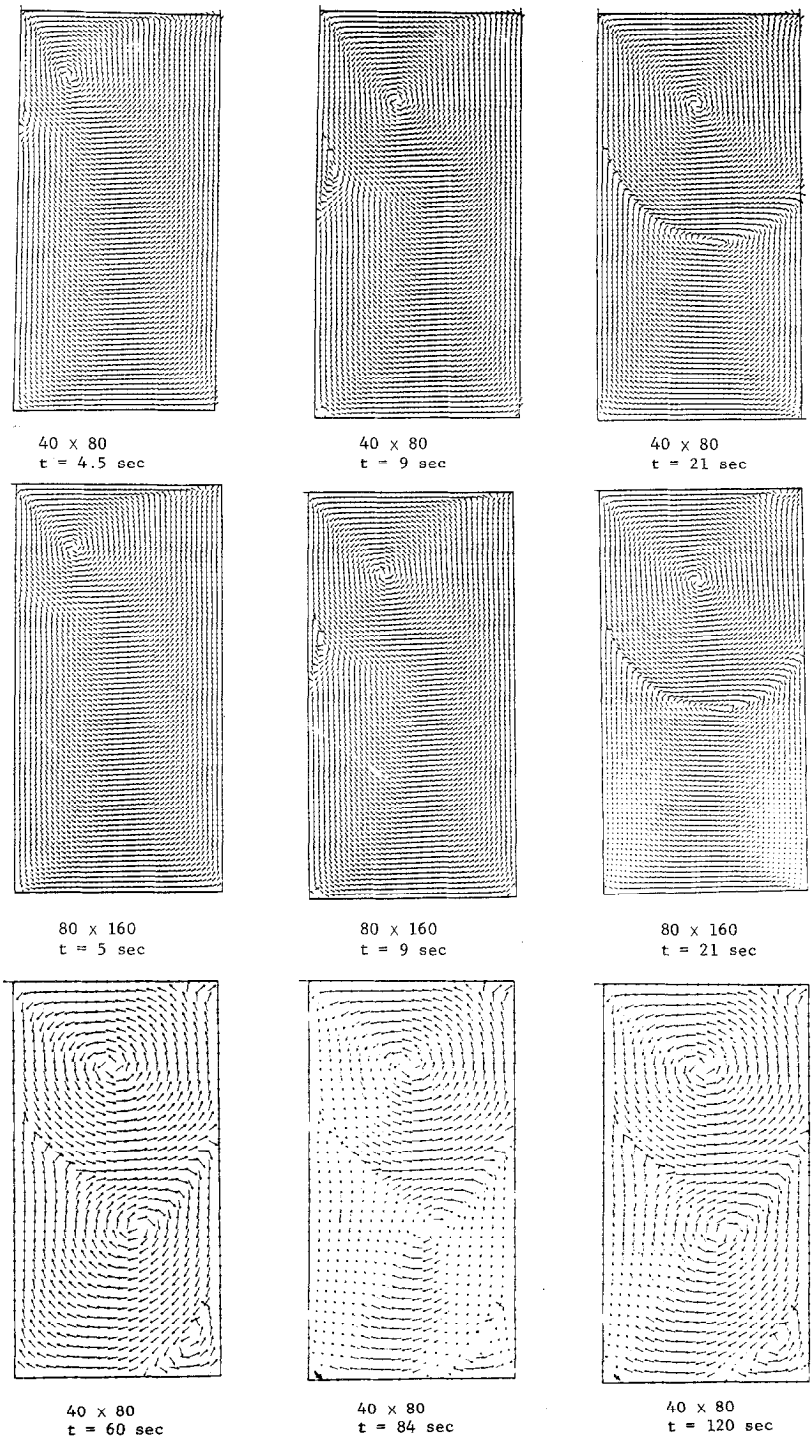

FIG. 2. Mesh size dependence at Re = 2000.

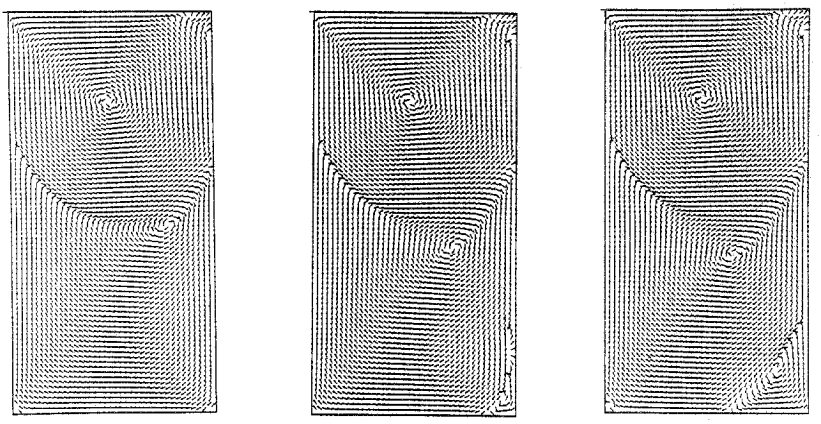

FIG. 2—*Continued.*

To investigate possible mesh-size dependence, prior to the main run at $\mathrm{Re} = 10{,}000$ we compared the 40×80 resolution with a finer grid 80×160 resolution at the lower Reynolds number $\mathrm{Re} = 2000$. See Fig. 2. Note that the finer grid did not generate a wall vortex until $t = 6$ sec whereas the coarse grid started the wall vortex at $t = 4.5$ sec. On the other hand once the initial data has propagated throughout the cavity, the finer grid flow features quickly catch up to those on the coarse grid. Some small variations occur thereafter. For example, the coarse grid fails to detect the beginning small action in the weaker lower left corner of the finer grid seen at $t = 30$ sec. In fact this small left corner vortex on the finer grid disappears at $t = 32$ sec, reappears at $t = 37$ sec, then disappears again until $t = 44$ sec when it reappears for good. At $t = 60$ sec the coarse grid has still not portrayed this small dynamical feature but does so at $t = 84$ sec. The "final" states of both grids are essentially the same, at $t = 60$ sec for the finer grid, $t = 120$ sec. for the coarse grid.

For later reference let us point out one other interesting feature of the flow at $\mathrm{Re} = 2000$. At this Reynold's number, the wall eddy develops after the principal vortex but before either corner vortex. Thereafter it merges, almost simultaneously, with the two corner vortices to generate the secondary principal vortex. See Fig. 3. This will not be the case at the higher Reynold's number $\mathrm{Re} = 10{,}000$.

Finally, the boundary layer thickness is

$$\delta \sim C\left(\frac{\nu x}{U(0)}\right)^{1/2} \sim C\,\mathrm{Re}^{-1/2} \tag{2.5}$$

up to a constant C. For flow impinging on a flat plate, for example, the constant C takes a value 4.99. If we direct principal interest to the flow down the left side of the cavity, regarded as basically an incoming vertical downward (with $U(0) \sim 1$) laminar flow instigated by the inertia imposed downward by the lid moving along

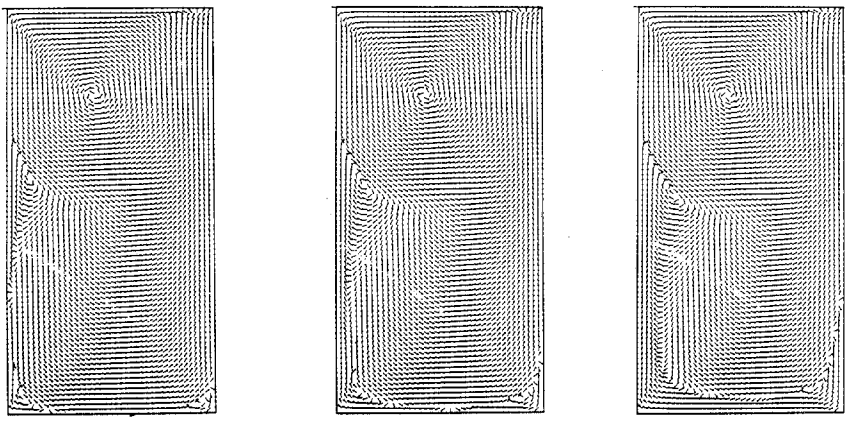

FIG. 3. Wall-corner dynamics at Re = 2000.

the top, at the left midwall ($x \sim 1$) at Re = 10,000 we would expect a boundary layer thickness of about $\delta \sim 5\ (10{,}000)^{-1/2} \sim 0.05$. Moreover, the much smaller flow velocities at left midwall create an effective local Reynolds number significantly smaller than 10,000. Thus we are able to resolve and capture the wall vortex dynamics reported herein.

3. TRANSIENT INITIAL DYNAMICS

In the remainder of the paper we consider only the flow simulation at aspect ratio $A = 2$ at the higher Reynolds number Re = 10,000.

The flow begins, see Fig. 4, much like all of those of [1] except that a small vortex splitting is already seen near the top at $t = 2$ sec. We regard this, which was also seen at Re = 2000, as a very short-lived transient off the principal vortex evolution. The eye of the principal vortex then descends the left (downstream) cavity wall until the formation of a wall eddy (approximately at depth 1) at $t = 10$ sec at which time it moves into the core of the cavity. This movement of the primary vortex is in sharp contrast to the analogous evolution observed at the lower Reynolds numbers Re $\leqslant$ 2000 wherein the eye entered the core upon formation.

The wall vortex is well formed at $t = 18$ sec but then starts to breakup at $t = 22$ sec prior to the development of either of the first lower corner vortices. Quickly the wall vortex splits, $t = 25$ sec, and at $t = 28$ sec we have a further split into three vortices in the interior separation region. At 34 sec one can discern, in fact, 4 subvortices.

Also at $t = 34$ sec, a second wall eddy formation can be observed on the right (upstream) wall of the cavity. This eddy will eventually become the upstream, cor-

ner-lid recirculation eddy. Note that this eddy forms at a time when the eye of the primary vortex is deepest. Thereafter the transient features of this eddy are its tendencies to separate or partially dissolve in accommodation with the primary vortex whose eye displays a (sometimes intense) oscillatory, vertical motion.

Concurrent to the formation of the lid-eddy is that of the secondary core vortex. This principal second region of recirculation has its origin in the left wall-eddy, a feature not characteristic of lower Reynolds number flows.

As mentioned in the previous section, see Fig. 3, at Reynolds number $\mathrm{Re} \leqslant 2000$ the secondary core vortex resulted from the fusion inside the interior of the cavity of the two corner eddies with (when it exists) the left wall-eddy. Here the secondary vortex detaches from the left wall-eddy ($t = 25$ sec), moves quickly across the width of the cavity to the right wall, and then back again into the interior before stopping at $t = 60$ sec. As in the case with lower Reynolds numbers the eye of the secondary vortex is displaced (the amount depending on the Reynolds number) toward the right cavity wall with respect to the eye of the primary vortex.

After the secondary vortex hits the right wall at $t \approx 40$ sec, a lower right corner-eddy forms, $t = 43$ sec. Then a left corner-eddy develops subsequent to the secondary vortex's retreat into the cavity's interior at $t \approx 58$. At this point (e.g., $t = 60$ sec) one can count 8 recirculation regions in the flow: two principal vortices, two vortices near the left midwall, the two lower corner-eddies, and the upper-right corner with its tertiary subeddy.

As the upper-left corner begins an attempted recirculation motion at $t = 60$ sec one can discern a simultaneous disintegration of the upper-right-corner flow into three small upper wall-eddies. However, this transient, presumably due to an "upwelling" action of the flow, soon disappears, $t = 65$ sec, as does the residual separation-region interaction.

continue to remain so due in part to the presence, in close proximity, of a wall eddy.

4. Intermediate Dynamics

After the onset dynamics in which the basic energy of the system is distributed throughout the cavity, the flow begins what we may roughly describe as a smoothing action. See Fig. 5. Although some qualitative tertiary action remains in the separation region near the left wall and in the upper-right corner, eventually most of it disappears. Note, however, the resemblance of the flow at $t = 110$ sec to that at 100 sec. The tertiary separation eddy near the left wall is seen only rarely after $t = 140$ sec. The flow pattern seen at $t = 140$ sec soon establishes itself as a basic one.

The flow during this intermediate interval $t = 70$ sec to $t = 140$ sec is dominated by a vertical oscillation of the eye of the principal vortex. As seen in Fig. 5, this

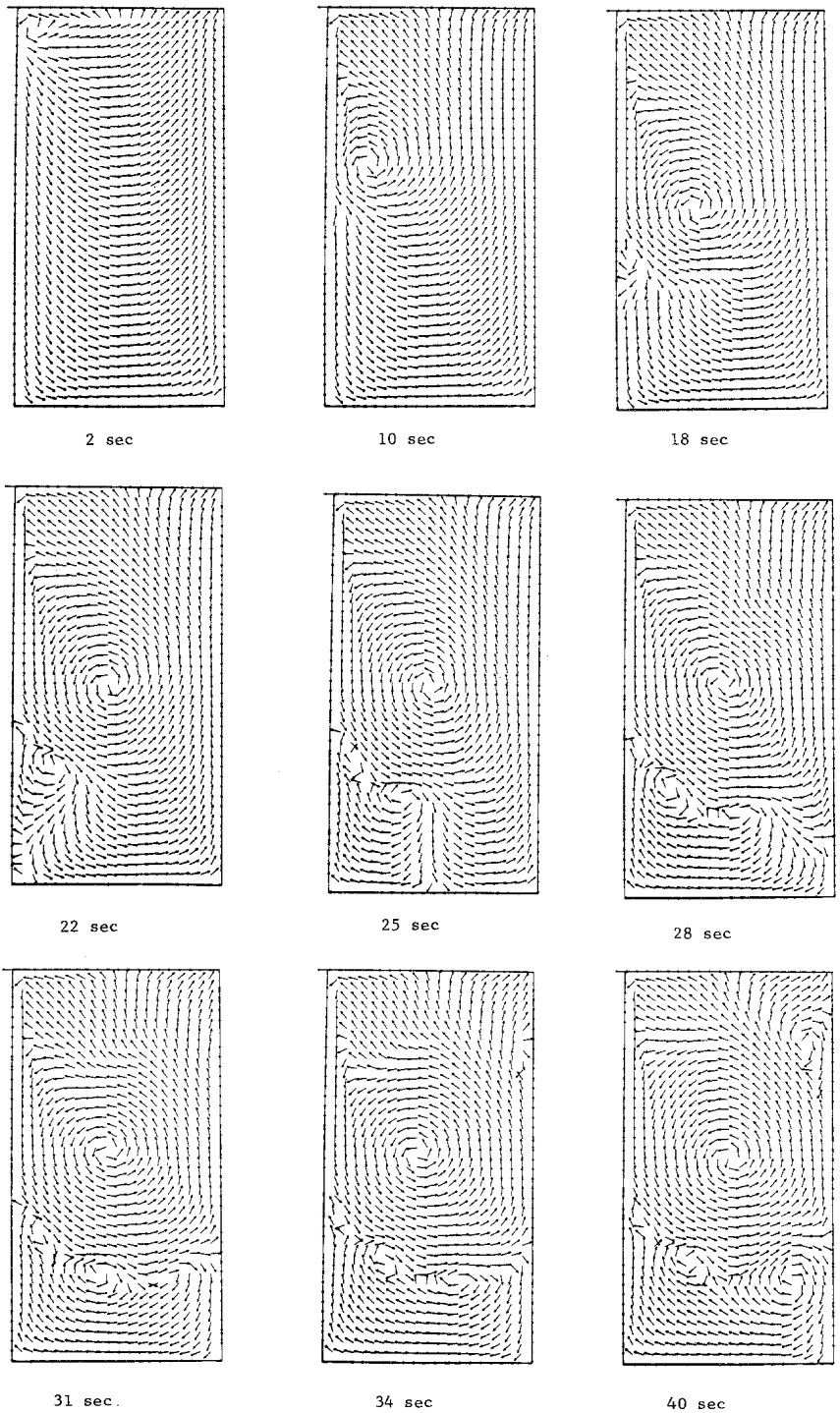

FIG. 4. Flow transients at Re = 10,000.

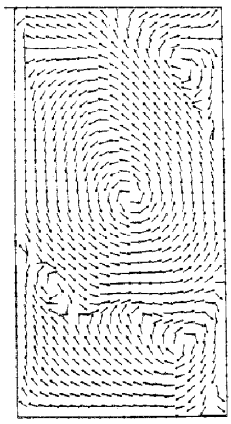

43 sec

48 sec

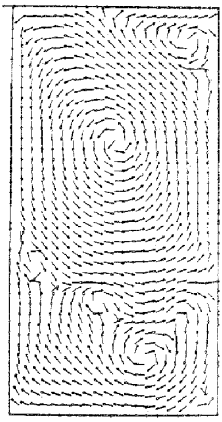

52 sec

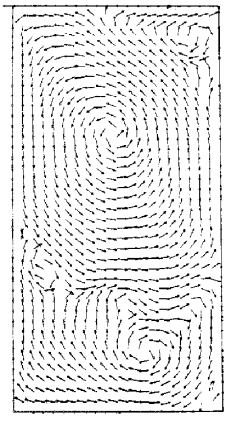

53 sec

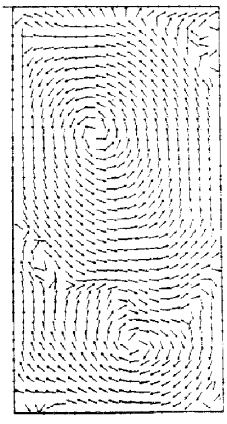

58 sec

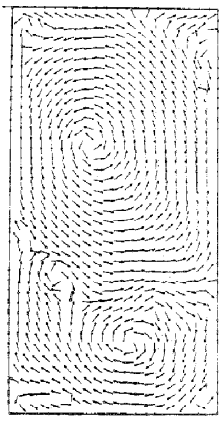

60 sec

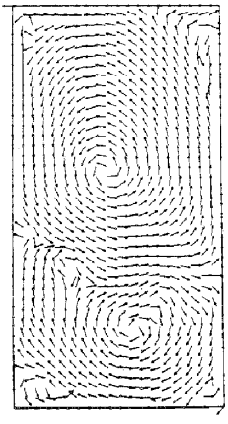

65 sec

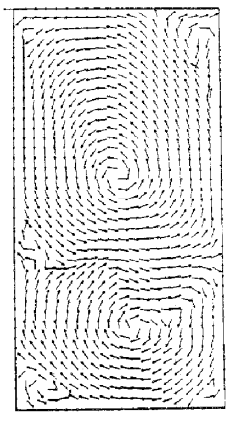

67 sec

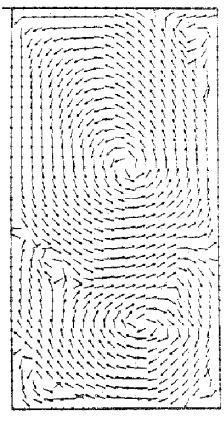

70 sec

FIG. 4—*Continued.*

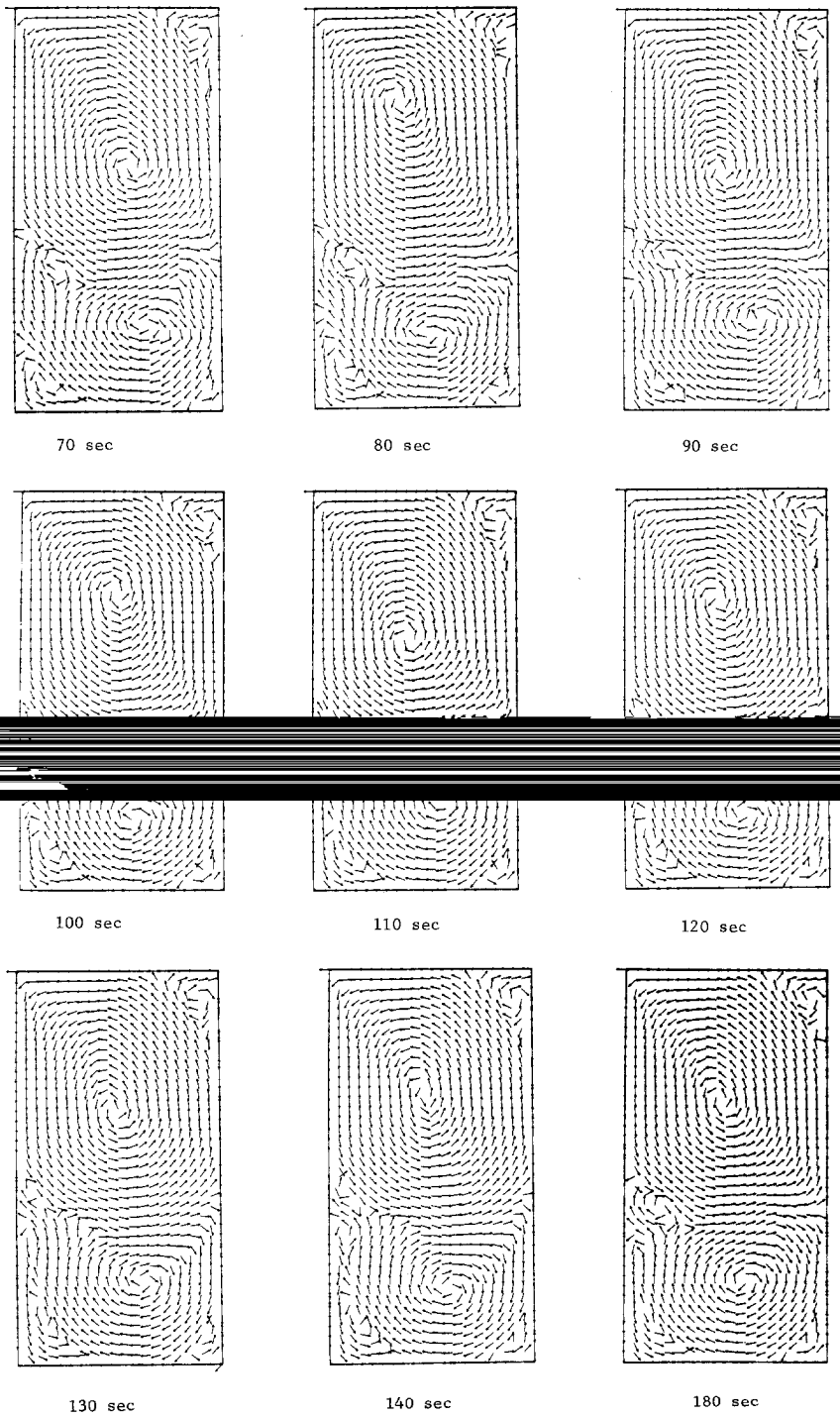

FIG. 5. Smoothing dynamics at Re = 10,000.

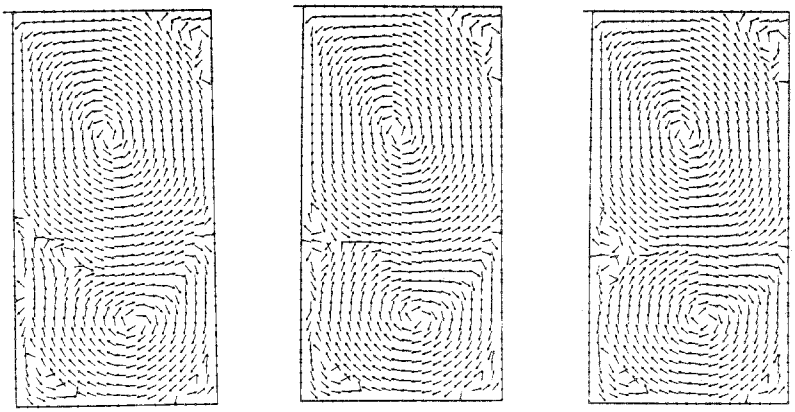

FIG. 6. Eventual smoothed flow at Re = 10,000.

movement is most intense between $t = 70$ sec and $t = 120$ sec. After $t = 140$ sec the location of the eye steadies.

The flow then continued to smooth the large scale vortex structures. See Fig. 6. Note the separation into upper- and lower-driven subcavities and the lack of significant change in secondary features except along the lower-left wall.

5. FINAL DYNAMICS

Although some smoothing continues from $t = 300$ sec to $t = 360$ sec (when we stopped the simulation), it is overshadowed by the persistent oscillation along the lower-left wall. While such oscillations have been seen in some thermally dependent flow simulations, we have not seen them in basic cavity flows. Nor did they occur in a unit cavity unsteady simulation at Re = 10,000 [4].

Figure 7 shows the patterns of this oscillation. In addition to the pronounced oscillation on the left, we note also very small tertiary nonstationarities at three points along the right wall: (i) just below the upper-right corner, where earlier there was a definite tertiary eddy; (ii) just below the right midwall, where the fluid separates into the upper and lower regions; (iii) at the top of the lower right corner-eddy. Whether or not these represent minor numerical or fluid instabilities or very small tertiary periodic final solutions are questions, in our opinion, secondary to whether the main oscillation along the lower-left wall represents a final periodic solution.

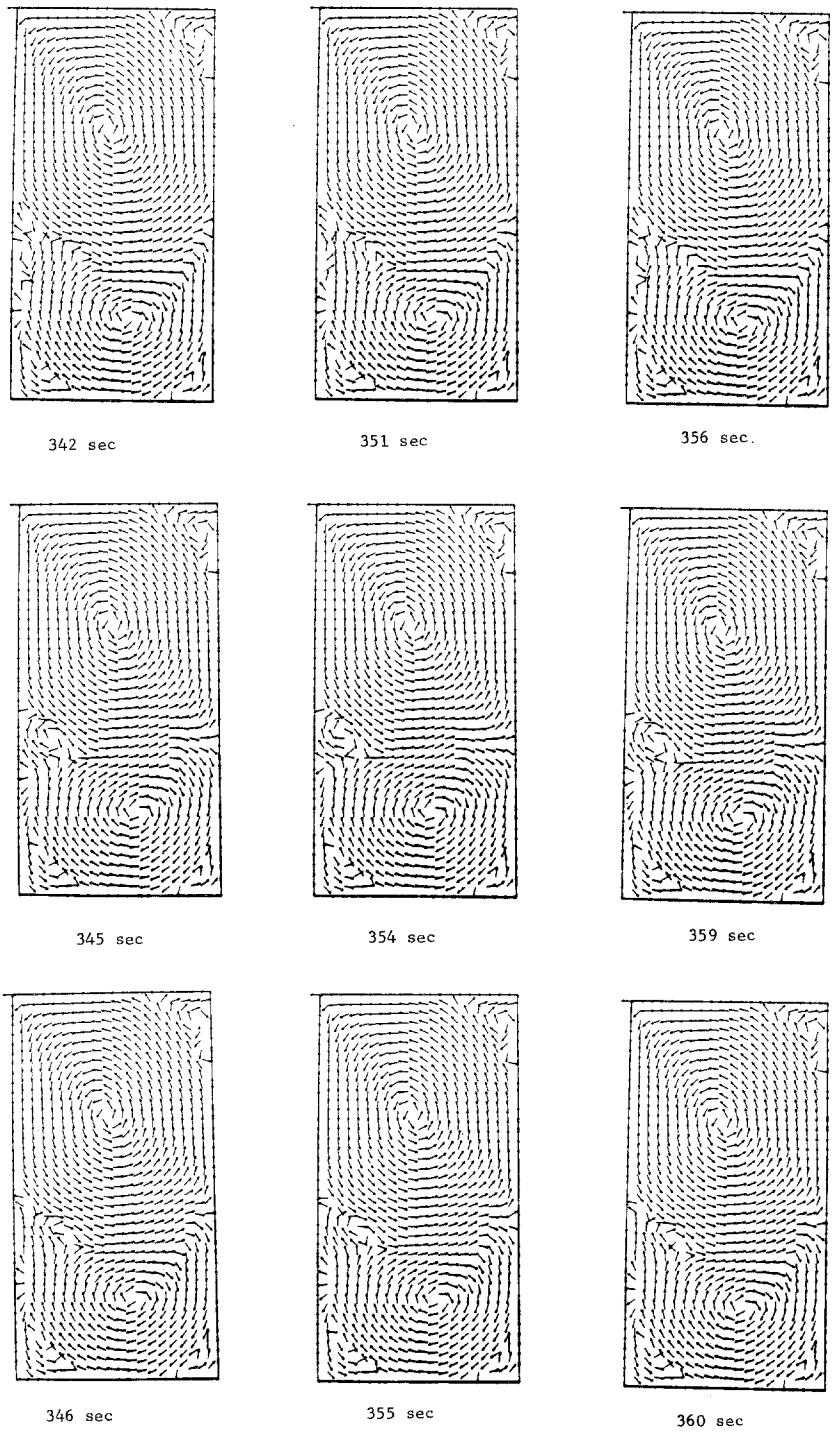

FIG. 7. Final oscillation at Re = 10,000.

6. Further Comments and Conclusions

Our results indicate a Hopf bifurcation, for flow in a depth 2 cavity, at some critical Reynolds number Re between 2000 and 10,000. One should distinguish this Hopf bifurcation of the discretized equations from the cases of the continuous equations and the actual physics. Moreover, the aspect ratio $A = \text{depth/width}$ enters as a second bifurcation parameter of considerable importance. That is, holding $\text{Re} = 10{,}000$ as reported herein, there is indicated a Hopf bifurcation at some critical A between 1 and 2.

Due to the multi-directional nature of the flow dynamics, any accurate incorporation of upwinding would result in a computational quagmire. On the other hand, in employing a forward Euler-MAC scheme, care is needed in choosing the discrete steps δt, δx, and δy to assure both stable time integration and adequate spatial resolution of the dynamics under consideration. We required that the ratio $4(\delta t)\, v/(\delta x)^2$ not exceed a critical value $K(v)$, where we have taken $\delta x = \delta y$. Because the equations are nonlinear, $K(v)$ must in general be determined experimentally by simulation runs on a coarse grid. For example, the value $v = 0.01$ yielded $K(v) \approx 1.0$, while $v = 0.0025$ yielded $K(v) \approx 0.36$. Our experiments with $K(v)$ indicated that $K(v) \to 0$ as $v \to 0$, in a non-linear way. Instability, when it occurred, manifested itself first in the downstream left lid-corner, resulting quickly in a subsequent dissolution of the primary vortex accompanied by a rapid buildup of large pressure gradients. On the other hand, a well-established primary vortex appeared to guarantee stability thereafter.

[redacted]

velocities near the midwall and corner vortex structures are considerably smaller than the driving velocity. For the $\text{Re} = 1/v = 10{,}000$ dynamics presented here, at the final time $t = 360$ sec, the effective local Reynold's number in the left-midwall region is about

$$(\text{Re})_{\text{effective}} \sim \frac{U_0^{\text{local}} L}{v} \leqq \frac{(0.1)(1)}{(10^{-4})} \sim 1000.$$

Examination of the velocity matrices during the whole time history revealed corresponding or smaller values in the neighborhoods of all secondary vortex structures. In particular, the transient wall vortex dynamics, i.e., separation point movement on the left wall, would appear to be accurately resolved.

References

1. K. Gustafson and K. Halasi, *J. Comput. Phys.* **64** (1986), 279–319.
2. R. Peyret and T. D. Taylor, *Computational Methods for Fluid Flow* (Springer, New York, 1983).
3. R. Temam, *Navier–Stokes Equations*, 3rd ed. (North–Holland, Amsterdam, 1985).
4. P. Gresho, S. Chan, R. Lee, and C. Upson, *Int. J. Numer. Methods Fluids* **4** (1984), 619–640.